1521-009X/50/5/541–551$35.00
DRUG METABOLISM AND DISPOSITION
dx.doi.org/10.1124/dmd.121.000783
Drug Metab Dispos 50:541–551, May 2022

Experimental and Modeling Evidence Supporting the *Trans*-Inhibition Mechanism for Preincubation Time-Dependent, Long-Lasting Inhibition of Organic Anion Transporting Polypeptide 1B1 by Cyclosporine A[S]

Saki Izumi, Yoshitane Nozaki, Wooin Lee, and Yuichi Sugiyama

Global Drug Metabolism and Pharmacokinetics, Tsukuba Research Laboratories, Eisai Co. Ltd., Tsukuba, Japan (S.I., Y.N.); College of Pharmacy and Research Institute of Pharmaceutical Sciences, Seoul National University, Seoul, Republic of Korea (W.L.); and Laboratory of Quantitative System Pharmacokinetics/Pharmacodynamics, Josai International University, Tokyo, Japan (Y.S.)

Received November 16, 2021; accepted February 14, 2022

ABSTRACT

Cyclosporine A (CsA) and rifampin are potent inhibitors of organic anion transporting polypeptide (OATP) 1B1 and are widely used to assess the risk for drug-drug interactions. CsA displays preincubation time-dependent, long-lasting inhibition of OATP1B1 in vitro and in rats in vivo, and a proposed mechanism is the *trans*-inhibition by which CsA inhibits OATP1B1 from the inside of cells. The current study aimed to experimentally validate the proposed mechanism using human embryonic kidney 293 cells stably expressing OATP1B1. The uptake of CsA reached a plateau following an approximate 60-minute incubation, with the cell-to-buffer concentration ratio of 3930, reflective of the high-affinity, high-capacity intracellular binding of CsA. The time course of CsA uptake was analyzed to estimate the kinetic parameters for permeability clearance and intracellular binding. When the OATP1B1-mediated uptake of [^{3}H]estradiol-17β-glucuronide was measured following preincubation with CsA for 5 to 120 minutes, apparent K_i values became lower with longer preincubation. Our kinetic modeling incorporated the two reversible inhibition constants [$K_{i,trans}$ and $K_{i,cis}$ for the inhibition from inside (*trans*-inhibition) and outside (*cis*-inhibition) of cells, respectively] and estimated $K_{i,trans}$ value of CsA was smaller by 48-fold than the estimated $K_{i,cis}$ value. Rifampin also displayed preincubation time-dependent inhibition of OATP1B1, albeit the extent of enhancement was only twofold. The current study provides experimental evidence for the preincubation time-dependent shift of apparent K_i values and a mechanistic basis for physiologically based pharmacokinetic modeling that incorporates permeability clearance, extensive intracellular binding, and asymmetry of K_i values between the inside and outside of cells.

SIGNIFICANCE STATEMENT

In vitro data and kinetic modeling support that preincubation time-dependent, long-lasting inhibition of OATP1B1 by CsA can be explained by the extensive intracellular binding and reversible OATP1B1 inhibition intracellularly (*trans*-inhibition) as well as extracellularly (*cis*-inhibition). For inhibitors to display time-dependency, the following factors were found important: time to reach a steady-state cellular concentration, *trans*-inhibition potency relative to *cis*-inhibition, and the degree of cellular inhibitor accumulation. This study would aid in the accurate prediction of drug-drug interactions mediated by OATP1B1 inhibition.

Introduction

Organic anion transporting polypeptide (OATP) 1B1 mediates the hepatic uptake of various anionic substrates, including many clinically important drugs (Niemi et al., 2011). When drug-drug interactions (DDIs) occur via mechanisms involving OATP1B1, the systemic exposure of OATP1B1 substrate drugs [e.g., 3-hydroxy-3-methylglutaryl coenzyme A reductase inhibitors (statins), angiotensin II receptor blockers, antidiabetic drugs, antihepatitis C virus drugs] increases by coadministration of the inhibitor drugs, such as cyclosporine A (CsA) and rifampin (Maeda, 2015; Lowjaga et al., 2020). In patients receiving statin therapy, DDIs can increase the systemic statin exposure and the risk of statin-related myotoxicity, including rare but severe rhabdomyolysis (Omar and Wilson, 2002; Neuvonen et al., 2006; Iwaki et al., 2019). To assess the potential risk of DDIs mediated by OATP1B1 inhibition, new chemical entities (NCEs) are routinely evaluated for their inhibition potency against OATP1B1 in vitro at the nonclinical stages.

Cell-based assays for OATP1B1 inhibition typically determine the half inhibitory concentration (IC_{50}) or the inhibition constant (K_i) for OATP1B1, key parameters in the prediction of DDI risk based on the static and dynamic models (Yoshida et al., 2012; Yoshikado et al., 2016; Taskar et al., 2020). In the conventional inhibition assays, a probe substrate of OATP1B1 is coincubated with an NCE (as a potential

dx.doi.org/10.1124/dmd.121.000783.
[S] This article has supplemental material available at dmd.aspetjournals.org.

ABBREVIATIONS: A, nonsaturable component for intracellular binding; CsA, cyclosporine A; DDI, drug-drug interaction; E_2G, estradiol-17β-glucuronide; f_T, intracellular unbound fraction; I_{buffer}, concentration of inhibitor in buffer; I_{cell}, total cellular concentration of inhibitor; K_d, dissociation constant; K_i, inhibition constant; $K_{i,app}$, apparent K_i value; $K_{i,cis}$, inhibition constant for *cis*-inhibition; $K_{i,trans}$, inhibition constant for *trans*-inhibition; $K_{p,uu}$, intracellular-to-buffer unbound drug concentration ratio; NTCP, Na+-taurocholate cotransporting polypeptide; OATP, organic anion transporting polypeptide; PBPK, physiologically based pharmacokinetics; PS_{act}, clearance via transporter-mediated active uptake; PS_{dif}, clearance via passive diffusion; SLC, solute carrier; $T_{1/2,max}$, time to reach half maximum intracellular concentration; TDI, time-dependent inhibition.

inhibitor). Several inhibitors, such as CsA, exhibit preincubation time-dependent, long-lasting inhibition of OATP1B1 in vitro (Amundsen et al., 2010; Shitara et al., 2012; Izumi et al., 2015). The inhibitory effect of CsA was sustained even after removing CsA from incubation buffer (Shitara et al., 2012; Furihata et al., 2014) and the inhibitory potency of CsA was enhanced with prolonged preincubation: apparent K_i ($K_{i,app}$) value was reduced by 3- to 22-fold compared with that determined without CsA preincubation (Amundsen et al., 2010; Gertz et al., 2013; Izumi et al., 2015). In addition, as shown in Supplemental Fig. 1, in vitro IC_{50} and/or K_i values obtained after CsA preincubation were comparable to in vivo K_i values estimated by physiologically based pharmacokinetic (PBPK) modeling of clinical DDI data (Yoshikado et al., 2016). Based on these findings, the latest regulatory DDI guidance/guidelines recommends considering the preincubation effects in the inhibition assays for OATP1B1 and OATP1B3 (MHLW, 2019; U.S. FDA, 2020).

Some practical approaches have been proposed to manage the time-dependent inhibition (TDI) of OATP1B1 in the DDI risk assessments (Izumi et al., 2015; Taguchi et al., 2020). However, the underlying mechanism has not been fully understood. A better understanding of the mechanisms contributing to the TDI of OATP1B1 may facilitate the incorporation of the TDI into PBPK modeling and quantitative prediction of OATP1B1-mediated DDIs. Consideration of the underlying mechanisms may also aid in the optimization of in vitro assay conditions for potential inhibitors of OATP1B1. Shitara and Sugiyama proposed that CsA can inhibit OATP1B1 not only from the outside (*cis*-inhibition) but also from the inside (*trans*-inhibition) of cells (Shitara and Sugiyama, 2017). Yet, supporting experimental data have been lacking.

This study investigated the TDI of OATP1B1 by CsA in human embryonic kidney (HEK) 293 cells stably expressing OATP1B1 (OATP1B1-HEK) and control cells (control-HEK), employing different assay conditions (Fig. 1). Rifampin was used for comparison as it is an OATP1B1 inhibitor with a modest preincubation time-dependent inhibitory effect (Pahwa et al., 2017; Barnett et al., 2018). The time profiles of cellular uptake and release were measured for CsA and rifampin in OATP1B1-HEK and control-HEK cells and analyzed by cellular kinetic modeling incorporating the *trans*-inhibition mechanism. The developed cellular kinetic models were also used to identify the factors contributing to the extent of TDI of OATP1B1.

Materials and Methods

Chemicals. [^{3}H]Estradiol-17β-glucuronide ([^{3}H]E_2G, 52.9 Ci/mmol) was purchased from PerkinElmer Life Sciences (Boston, MA), and unlabeled E_2G and rifampin were purchased from Sigma-Aldrich (St. Louis, MO). CsA was obtained from Toronto Research Chemicals (Toronto, ON, Canada). All other chemicals were of analytical grade and commercially available.

Cell Culture. OATP1B1-HEK and control-HEK were established previously (Izumi et al., 2013). The cells were seeded in the poly-D-lysine-coated 48-well plate (BD Bioscience, San Jose, CA) at the density of 2×10^5 cells/well and cultured for 48 hour at 37°C under 5% CO_2 gas in a humidified incubator.

Inhibition of OATP1B1 by CsA and Rifampin in OATP1B1-HEK Cells. Fig. 1 depicts the four different inhibition assay conditions used to respectively capture *cis*-, *trans*-, both *cis*- and *trans*-inhibition (*cis*+*trans*-inhibition), and long-lasting inhibition by CsA or rifampin using OATP1B1-HEK and control-HEK. Using [^{3}H]E_2G (0.1 μM) as a probe substrate for OATP1B1 (Izumi et al., 2013), the initial uptake was assessed for 1 minute. Unless noted otherwise, Krebs Henseleit (KH) buffer (118 mM of NaCl, 23.1 mM of $NaHCO_3$, 4.83 mM of KCl, 0.96 mM of KH_2PO_4, 1.20 mM of $MgSO_4$, 12.5 mM of HEPES, 5.0 mM of glucose, and 1.53 of mM $CaCl_2$, pH 7.4) was used for cell incubation (500 µl/well) and washing (1 ml/well), and incubations were performed at 37°C. For the long-lasting inhibition conditions, 50 µl of KH buffer was collected after the washout period to measure the inhibitor concentrations

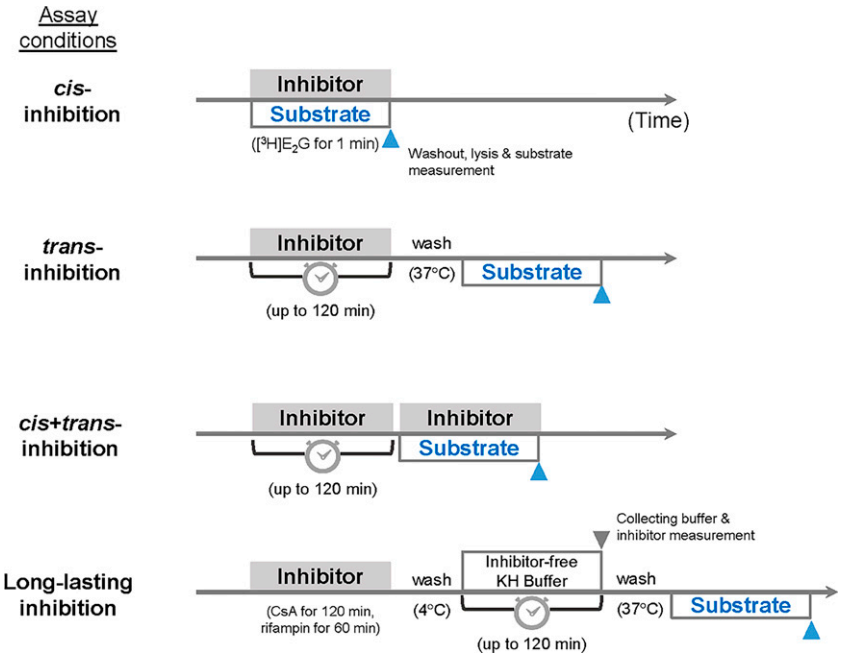

Fig. 1. Different inhibition assay conditions employed in the current study. In the *cis*-inhibition assay, a substrate and an inhibitor were simultaneously added to cells and coincubated without preincubation of the inhibitor. Since the distribution of inhibitors into cells was minimal, inhibitors can inhibit OATP1B1 from the outside of cells (*cis*-inhibition). In the *trans*-inhibition assay, cells were preincubated with an inhibitor before examining the uptake of a probe substrate. After washing cells, the uptake of the probe substrate was examined in the absence of the inhibitor in buffer. In this condition, inhibitors remaining in the cells can inhibit OATP1B1 from the inside of cells (*trans*-inhibition). In the *cis*+*trans*-inhibition assay, the assay flow was consistent with that of *trans*-inhibition, except for coincubation of the probe substrate and inhibitor after the inhibitor preincubation step. Under this assay condition, the inhibitor can inhibit OATP1B1 from both outside (*cis*-inhibition) and inside (*trans*-inhibition) of cells. In long-lasting inhibition assay, cells were preincubated with inhibitors for designated time period, followed by washout and incubation with fresh KH buffer at 37°C. At the designated times, cells were washed again, and the uptake of a probe substrate was examined in the absence of the inhibitor to monitor the recovery of OATP1B1 activity.

released from the cells at the designated times (10, 30, 60, and 120 minutes for CsA; 10 and 60 minutes for rifampin). For all the assay conditions, cells were washed with ice-cold KH buffer twice at the end of the substrate uptake and stored at –20°C until sample processing for measurement of the cellular concentrations of the probe substrate.

Uptake and Release Assays for CsA and Rifampin Using OATP1B1-HEK Cells

For the uptake (for CsA and rifampin) and release assays (for CsA), OATP1B1-HEK and control-HEK cells were preincubated with prewarmed KH buffer for 5 minutes at 37°C. For the uptake assay, the preincubation buffer was removed, and, subsequently, the uptake reaction was initiated by adding 500 µl of a prewarmed KH buffer containing CsA or rifampin. At the designated time, 50 µl of assay buffer was collected to measure the drug concentrations in buffer. After removing the residual buffer, cells were immediately washed with 1 ml of ice-cold KH buffer twice. For the release assay for CsA, cells were incubated with CsA for 120 minutes. After removing the incubation buffer and washing cells, 500 µl of prewarmed KH buffer was added, and cells were incubated for up to 30 minutes at 37°C. At the designated times (up to 30 minute), 50 µl of incubation buffer was collected, and cells were washed with 1 ml of ice-cold KH buffer twice. Cells were plated in triplicate wells for sample collection at each timepoint. Both buffer and cellular samples were stored at –20°C until sample processing to measure CsA and rifampin.

Quantification of [^{3}H]E_2G, CsA, and Rifampin. To measure cellular radioactivity of [^{3}H]E_2G, cells were lysed with 200 μl of 0.1 N NaOH, and the resulting cell lysate was neutralized with 20 μl of 1 N HCl. An aliquot (150 μl) of the neutralized cell lysate was mixed with 2 ml of scintillation fluid (Hionic-Fluor; Perkin Elmer Life Sciences), and the radioactivity was measured by a liquid scintillation counter (LSC; Tri-Carb A5110TR, PerkinElmer Life Sciences). The remaining neutralized cell lysate samples were used to quantify the protein concentrations using a BCA Protein Assay Kit (Thermo Fisher Scientific, Waltham, MA). For buffer samples, 20 μl of the aliquot was mixed with 2 ml of scintillation fluid to measure the radioactivity by the LSC.

To measure unlabeled CsA and rifampin taken up by OATP1B1-HEK and control-HEK, the cells were vigorously mixed and deproteinized using 300 μl of methanol containing an appropriate internal standard, followed by filtration and analysis via liquid chromatography coupled with tandem mass spectrometry (LC-MS/MS). To quantify CsA and rifampin in KH buffer, 50 μl of the aliquot was mixed with 200 μl of methanol containing an appropriate internal standard and injected to LC-MS/MS. Protein assay was performed as described above for cells seeded in extra wells.

The LC-MS/MS system consisted of an AQUITY UPLC I-Class System (Waters Corp.), Xevo TQ-XS (Waters Corp.), and MassLynx Mass Spectrometry Software (version 4.2; Waters Corp.). For the analysis of CsA, chromatographic separation was performed using a Waters Acquity UPLC BEH C18 column (1.7 μm, 2.1 mm i.d., 30 mm; Waters, Milford, MA) at 65°C. The mobile phases were composed of distilled water containing 0.1% formic acid (solvent A) and acetonitrile containing 0.1% formic acid (solvent B), and the initial condition was 98% solvent A at a flow rate of 0.4 ml/min. After maintaining the initial condition for 0.5 minutes, solvent B was linearly increased to 80% over 1.5 minutes with a 1-minute hold at 80% B. For rifampin, the same UPLC column and mobile phases were used. The column temperature and flow rate were set to 40°C and 0.3 ml/min, respectively. The initial condition was 98% solvent A, and B was linearly increased to 80% over 3 minutes, then to 100% over the next 0.01 minutes with a 0.5-minute hold at 100% B. The column was equilibrated with the initial mobile phase before each injection (injection volume, 1 μl). The analytes were detected by electrospray ionization in positive ion mode, and the selected ion monitoring transitions were: 1202.8 > 224.1 for CsA and 823.46 > 791.09 for rifampin.

Kinetic Modeling

Data fitting was performed by a nonlinear least-squares regression method using Napp version 2.31 (Hisaka and Sugiyama, 1998).

Kinetic Analysis of Cellular Uptake and Inhibition in OATP1B1-HEK and Control-HEK cells. The OATP1B1-mediated uptake clearance of a substrate was calculated by subtracting the uptake clearance in control-HEK from that in OATP1B1-HEK. The apparent inhibition constant ($K_{i,app}$) value was estimated for CsA and rifampin by examining their inhibitory effects on the OATP1B1-mediated uptake of a probe substrate (% of control), using the following equation:

$$\%\ \text{of control} = 100/(1 + I_{buffer}/K_{i,app}) \quad (1)$$

where I_{buffer} represents the nominal concentrations of inhibitors in buffer (μM) and $K_{i,app}$ is an inhibition constant based on the I_{buffer} values. Concentration-dependent uptake of a substrate via OATP1B1 was examined with or without an inhibitor and was analyzed by the Michaelis-Menten equation:

$$v = \frac{V_{max} \times S}{K_m + S} \quad (2)$$

where v, S, V_{max}, and K_m represent the uptake velocity (pmol/min/mg protein), substrate concentration (μM), the maximum uptake velocity (pmol/min/mg protein), and Michaelis constant (μM), respectively.

Saturation of Intracellular Binding of CsA in HEK293 Cells. Concentration-dependent uptake of CsA by OATP1B1-HEK and control-HEK was determined at 120 minutes after incubation and analyzed by the following equation to estimate parameters for the intracellular binding:

$$I_{cell} - I_{buffer} = (B_{max} \times I_{buffer})/(K_d + I_{buffer}) + A \times I_{buffer} \quad (3)$$

where I_{cell} and I_{buffer} represent the measured values for the total cellular and buffer concentration of CsA (μM), respectively. As no active transport process was implicated for CsA in OATP1B1-HEK or control-HEK, the cellular unbound concentration of CsA (a neutral compound) was assumed to be equal to its concentration in buffer (I_{buffer}) at the steady-state. The cellular bound concentration of CsA can be obtained by (I_{cell}–I_{buffer}) at steady-state. K_d, B_{max}, and A represent the dissociation constant (μM), the maximum number of binding sites per cellular volume (μM), and nonsaturable component for intracellular CsA binding, respectively. To calculate I_{cell} from the uptake data, the cellular volume of HEK293 cells was set to 2 µl/mg protein according to a previous report (Shitara and Sugiyama, 2017).

Modeling of Cellular Pharmacokinetics of CsA and Rifampin. For the observed time profiles of the uptake and release of CsA and rifampin determined in OATP1B1-HEK and control-HEK, the clearances via OATP1B1-mediated active uptake (PS_{act}, µl/min/mg protein) and via passive diffusion (PS_{dif}, µl/min/mg protein) were estimated by simultaneously fitting to the following equations:

$$V_{cell} \cdot PA \cdot \frac{dI_{cell}}{dt} = (PS_{act} + PS_{dif}) \cdot PA \cdot I_{buffer} - PS_{dif} \cdot PA \cdot f_T \cdot I_{cell} \quad (4)$$

$$V_{buffer} \cdot \frac{dI_{buffer}}{dt} = -(PS_{act} + PS_{dif}) \cdot PA \cdot I_{buffer} + PS_{dif} \cdot PA \cdot f_T \cdot I_{cell} \quad (5)$$

where V_{cell}, V_{buffer}, PA, and f_T represent the cellular volume of HEK293 cells (2 μl/mg protein), the volume of incubation buffer (500 μl/well), the protein amount per well (mg protein/well), and intracellular unbound fraction, respectively. PS_{act} was set to zero based on the lack of evidence supporting CsA as a substrate of OATP1B1. Rifampin is known to be an OATP1B1 substrate, and PS_{act} was defined by the following equation:

$$PS_{act} = \frac{V_{max}}{K_m + S} \quad (6)$$

The intracellular binding of rifampin appeared constant in HEK293 cells in the tested concentration range (data not shown), but nonlinearity was observed for CsA. Therefore, f_T (I_{buffer}/I_{cell}) of CsA was described by the following equation, derived from Eq. 3.

$$f_T = \left[\sqrt{(B_{max} + (1+A) \cdot K_d - I_{cell})^2 + 4 \cdot (1+A) \cdot K_d \cdot I_{cell}} - \{B_{max} + (1+A) \cdot K_d - I_{cell}\}\right] / \{2 \cdot (1+A) \cdot I_{cell}\} \quad (7)$$

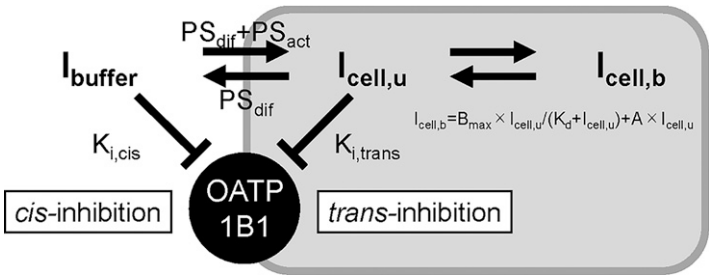

Fig. 2. Diagram depicting *cis*- and *trans*-inhibition of OATP1B1 in vitro. In this model, an inhibitor (I) in buffer (I_{buffer}) enters cells by passive diffusion (PS_{dif}) with or without transporter-mediated active uptake (PS_{act}), and inhibits OATP1B1 from both outside (*cis*-inhibition) and inside (*trans*-inhibition) of cells. $K_{i,cis}$ represents the inhibition constant for the *cis*-inhibition of OATP1B1 based on the I_{buffer}. $K_{i,trans}$ represents the inhibition constants for the *trans*-inhibition of OATP1B1 based on the intracellular unbound concentration ($I_{cell,u}$). Intracellular unbound fraction (f_T) is set constant (rifampin) or nonlinear (CsA). For the inhibitor that shows nonlinear f_T, the intracellular bound concentration ($I_{cell,b}$) is saturable with K_d (dissociation constant), B_{max} (maximum number of binding sites for intracellular binding), and A (nonsaturable component).

Mechanism for Time-Dependent Inhibition of OATP1B1. Fig. 2 depicts our proposed mechanism for TDI of OATP1B1, which is inhibited reversibly not only from the outside (*cis*-inhibition), but also from the inside (*trans*-inhibition) of cells (Shitara and Sugiyama, 2017). Based on our in vitro results using CsA, the competitive inhibition was applied to *cis*-inhibition, while the noncompetitive inhibition to *trans*-inhibition (detailed description in the "Results" section) also for rifampin. The following equation describes OATP1B1-mediated uptake clearance of a probe substrate in the presence of an inhibitor ($CL_{OATP1B1+I}$):

$$CL_{OATP1B1+I} = \frac{{}^{V_{max}}/\left(1+{}^{f_T \cdot I_{cell}}/_{K_{i,trans}}\right)}{K_m \cdot \left(1+{}^{I_{buffer}}/_{K_{i,cis}}\right)+S} \quad (8)$$

where $K_{i,cis}$ is the inhibition constant (μM) for *cis*-inhibition defined by the extracellular unbound concentration, and $K_{i,trans}$ is the inhibition constant (μM) for *trans*-inhibition defined by intracellular unbound concentration. As the substrate concentration used in our inhibition assays ([^{3}H]E_2G, 0.1 μM) was much lower than the reported K_m value (7.0 μM) (Izumi et al., 2013), the changes in OATP1B1-mediated uptake clearance (expressed as % of control) were approximated as follows (Shitara and Sugiyama, 2017):

$$\%\ \text{of control} = 100/\left[\left(1+{}^{I_{buffer}}/_{K_{i,cis}}\right)\cdot\left(1+{}^{f_T \cdot I_{cell}}/_{K_{i,trans}}\right)\right] \quad (9)$$

For the *cis*-inhibition assay conditions, the $K_{i,app}$ value (Eq. 1) corresponds to the $K_{i,cis}$ value as the I_{cell} value is zero. For the *trans*-inhibition and long-lasting inhibition assay conditions, the I_{buffer} was set to zero as the buffer containing an inhibitor was removed before initiating [^{3}H]E_2G uptake.

Statistical Analysis. The data were presented as mean ± S.E.M. or SD. The Student's two-tailed unpaired *t* test was used for group comparison (GraphPad Prism 9, GraphPad Software, La Jolla, CA). The differences were considered statistically significant when $P < 0.05$.

Results

Preincubation Time-Dependent Inhibition of OATP1B1 by CsA in OATP1B1-HEK Cells. The inhibitory effect of CsA on OATP1B1-mediated uptake of [^{3}H]E_2G was examined in the *cis*-, *trans*-, and *cis*+*trans*-inhibition conditions using OATP1B1-HEK and control-HEK (Fig. 3 and Table 1). In the *cis*-inhibition condition, CsA inhibited OATP1B1-mediated uptake of [^{3}H]E_2G in a concentration-dependent manner with $K_{i,app}$ (= $K_{i,cis}$) of 0.297 μM (Fig. 2). In the *trans*- and *cis*+*trans*-inhibition conditions, CsA inhibited the OATP1B1 activity more potently than in the *cis*-inhibition condition. When the preincubation time was varied (10 versus 120 minutes), the inhibitory potency of CsA increased with a longer preincubation time (Fig. 3 and Table 1): $K_{i,app}$ values for the *trans*-inhibition conditions, 0.0523 and 0.0169 μM after 10- and 120-minute preincubation with CsA; $K_{i,app}$ values for the *cis*+*trans*-inhibition conditions, 0.0378 and 0.0109 μM after 10- and 120-minute preincubation with CsA.

Inhibition Types for *Cis*- and *Trans*-Inhibition of OATP1B1 by CsA. The inhibition types for *cis*- and *trans*-inhibition of OATP1B1 by CsA were examined by preparing the Eadie-Hofstee plots, as shown in Fig. 4. In the *cis*-inhibition condition [cells were coincubated with [^{3}H]E_2G (0.02–100 μM) and CsA (0.3 μM); no preincubation with CsA], the K_m value increased from 8.52 to 16.9 μM, but there was no change in V_{max} (Table 2). In the *trans*-inhibition condition [the uptake of [^{3}H]E_2G (0.02–100 μM) was measured after 60-minute preincubation with CsA (0.01 μM)], the V_{max} decreased from 241 to 167 pmol/min/mg protein, but there was no change in K_m (Table 2). These results indicated that CsA inhibited OATP1B1 competitively from the outside and noncompetitively from the inside of cells.

Concentration-Dependent Uptake of CsA into HEK293 Cells. The time-dependent uptake of CsA was similar between OATP1B1-HEK and control-HEK, in line with CsA being a nonsubstrate of OATP1B1 (Fig. 5A). The uptake of CsA reached an apparent plateau around 60–120 minutes. The CsA uptake normalized by the medium concentration (μl/mg protein) at 0.1 μM was approximately 3.5-fold greater than that at 10 μM at 120 minutes after incubation.

When the concentration-dependent uptake of CsA was further analyzed at 120 minutes after incubation in OATP1B1-HEK and control-HEK (Fig. 5B), the cellular uptake of CsA appeared to contain both saturable and nonsaturable components, with nearly overlapping profiles

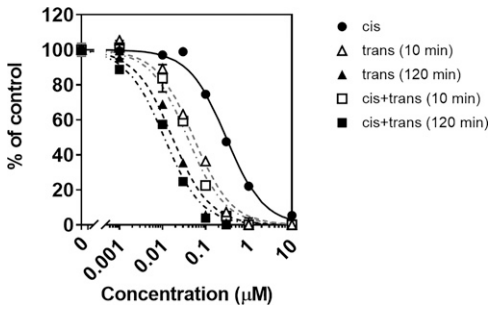

Fig. 3. Inhibitory effect of CsA on OATP1B1-mediated uptake of [^{3}H]E_2G under *cis*-, *trans*-, and *cis*+*trans*-inhibition conditions in OATP1B1-HEK cells. In the *cis*-inhibition condition, CsA (0.001–10 μM) and [^{3}H]E_2G (0.1 μM) were coincubated without preincubation with CsA (●). In the *trans*-inhibition condition, [^{3}H]E_2G uptake was examined after 10- (△) or 120-min (▲) preincubation with CsA. In the *cis*+*trans*-inhibition condition, CsA and [^{3}H]E_2G were coincubated after 10- (□) or 120-min (■) preincubation with CsA. Each symbol represents mean ± S.E.M. (n = 3), and solid (*cis*-inhibition), dash (*trans*-inhibition), and dash-dotted lines (*cis*+*trans*-inhibition) represent fitted lines according to Eq. 1. See also Fig. 1 for details of assay conditions.

TABLE 1

$K_{i,app}$ values of CsA and rifampin for OATP1B1 in *cis*-, *trans*-, or *cis*+*trans*-inhibition conditions in OATP1B1-HEK cells.
The inhibitory effect of CsA and rifampin on OATP1B1-mediated uptake of [^{3}H]E_2G (0.1 μM) was examined in *cis*-, *trans*-, or *cis*+*trans*-inhibition assays (Figs. 3, 7, *and* 9) according to Fig. 1. Each experiment was performed in triplicate and repeated at least twice. The observed $K_{i,app}$ values were estimated by a nonlinear least-squares regression analysis by using *Eq. 1* and presented as parameter estimate ± parameter SD.

Inhibitors	Preincubation Time (min)	Observed $K_{i,app}$ (μM)		
		cis-inhibition	*trans*-inhibition	*cis*+*trans*-inhibition
CsA	0	0.297 ± 0.027	NA	NA
	5	NA	0.217 ± 0.051	NT
	10	NA	0.0688 ± 0.0114	0.0378 ± 0.0042
	30	NA	0.0371 ± 0.0153	NT
	60	NA	0.0211 ± 0.0046	NT
	120	NA	0.0180 ± 0.0017	0.0109 ± 0.0011
Rifampin	0	1.16 ± 0.01	NA	NA
	10	NA	1.39 ± 0.09	0.492 ± 0.027
	60	NA	1.01 ± 0.13	0.524 ± 0.065

NA, not applicable; NT, not tested.

between OATP1B1-HEK and control-HEK. The observed data (from OATP1B1-HEK and control-HEK cells) was fitted to a cellular kinetic model incorporating the saturable intracellular binding (Eq. 3). The obtained parameters were K_d of 0.0914 μM, B_{max} of 326 μM, and non-saturable component (A) of 362 (Table 3). Under the linear condition, the f_T value and cell-to-medium CsA concentration ratio were calculated to be 0.000254 and 3930, respectively. CsA was reported to strongly bind with a 1:1 stoichiometry to cyclophilin A (Ke et al., 1994), a pharmacological target of CsA ubiquitously expressed in the body (Ryffel et al., 1991). Cyclophilin A accounted for as much as 0.1–0.4% of the total protein (28.6–114 μM) (Marks et al., 1991; Ryffel et al., 1991; Sarris et al., 1992), and the reported K_d values of CsA for cyclophilin A ranged from 0.013 to 0.03 μM (Dalgarno et al., 1986; Quesniaux et al., 1988; Kuglstatter et al., 2011), which were within a few folds difference compared with the currently observed B_{max} (326 μM) and K_d (0.0914 μM) values in HEK293 cells, respectively (Table 3).

Kinetic Modeling of Time-Dependent Inhibition of OATP1B1 by CsA in OATP1B1-HEK Cells. Similar profiles were observed for the uptake and release of CsA between OATP1B1-HEK and control-HEK. As such, the data were combined and analyzed by the cellular kinetic model incorporating the saturable intracellular binding of CsA (Fig. 6). The time profiles for the uptake and release of CsA were well captured by the cellular kinetic model using the observed intracellular binding parameters, yielding the estimated PS_{dif} value of 87.8 ± 9.0 μl/min/mg protein.

To estimate $K_{i,trans}$ of CsA for OATP1B1, the effect of CsA preincubation time on the potentiation of OATP1B1 inhibition was further analyzed in the *trans*-inhibition condition (Fig. 7). With prolonged preincubation with CsA (for 5 to 120 minutes), the inhibitory effect of CsA on OATP1B1-mediated uptake of [^{3}H]E_2G was enhanced, reaching the maximal inhibition with 60-minute or longer preincubation (Fig. 7, A and B). The observed data were well captured by the cellular kinetic model with the estimated PS_{dif} and $K_{i,trans}$ values of 51.3 μl/min/mg protein and 0.00619 μM, respectively (Table 3): the simulated profiles are shown in solid lines and in good agreement with the observed data in Fig. 7, A and B. The current model for CsA with the optimized parameters (Table 3) well captured the preincubation time-dependent shift of $K_{i,app}$ (defined with regard to the initial medium concentration) observed under the *trans*-inhibition conditions ($K_{i,app,trans}$) as shown in Fig. 7C.

For long-lasting inhibition assay conditions, the recovery of OATP1B1 activity was monitored after preincubation with CsA (120 minutes), followed by the incubation with CsA-free KH buffer (up to 120 minutes), using OATP1B1-HEK and control-HEK (Fig. 8A).The release of CsA and recovery of OATP1B1 activity were well captured by the cellular kinetic model (simulated profiles in solid and dotted lines in Fig. 8, B and C, respectively) using the estimated parameters in Table 3.

Kinetic Modeling of Time-Dependent Inhibition of OATP1B1 by Rifampin in OATP1B1-HEK Cells. When the time profiles for the uptake of rifampin was examined at 0.1, 0.3, 1, 2, 5, and 10 μM using OATP1B1-HEK and control-HEK, the uptake of rifampin reached the steady-state promptly, within 10 minutes, and the OATP1B1-mediated uptake was fully saturated at 10 μM (Supplemental Fig. 2). Since control-HEK cells were used in this study, f_T value could be estimated as well as PS_{dif}, V_{max}, and K_m values. The obtained data were simultaneously fitted to the cellular kinetic model, yielding the PS_{dif}, V_{max}, K_m, and f_T values of 52.5 μl/min/mg protein, 25.1 pmol/min/mg protein, 0.382 μM, and 0.0311, respectively (Table 3).

The inhibitory effect of rifampin on OATP1B1-mediated uptake of [^{3}H]E_2G was examined in the *cis*-, *trans*-, and *cis*+*trans*-inhibition conditions (Fig. 9A). In the *cis*-inhibition conditions, the $K_{i,app}$ value (corresponding to $K_{i,cis}$ in Fig. 2) of rifampin was 1.16 μM. *Trans*-inhibition assay conditions after 10- and 60-minute preincubation with rifampin yielded $K_{i,app}$ values of 1.39 and 1.01 μM, respectively, comparable to those in the *cis*-inhibition condition. The *cis*+*trans*-inhibition assay conditions gave slightly more potent inhibition of OATP1B1 with the

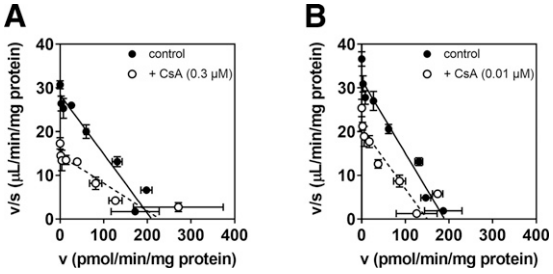

Fig. 4. Eadie-Hofstee plots to assess the inhibition types for *cis*- and *trans*-inhibition of OATP1B1 by CsACsA in OATP1B1-HEK cells. The concentration dependent uptake of [^{3}H]E_2G (0.002 – 100 μM) for 1 min at 37°C was investigated in *cis*- (A) and *trans*-inhibition (B) conditions. (A) OATP1B1-mediated uptake of [^{3}H]E_2G was investigated in the absence (●) or presence (○) of CsA (0.3 μM) without preincubation step with CsA. (B) Cells were preincubated for 60 min in the absence (●) or presence (○) of CsA (0.01 μM). After washing, OATP1B1-mediated uptake of [^{3}H]E_2G was investigated in the absence of CsA. The concentration-dependent uptake of E_2G was analyzed by Eq. 2 and the data are shown as an Eadie-Hofstee plot. Representative data from three independent experiments are presented, and each point represents mean ± S.E.M. (n = 3).

TABLE 2

Concentration dependence of OATP1B1-mediated uptake of [^{3}H]E_2G in the presence and absence of CsA under *cis*- and *trans*-inhibition assay conditions. OATP1B1-mediated uptake of [^{3}H]E_2G (0.002 – 100 μM) was examined in the presence and absence of CsA (0.3 and 0.01 μM for *cis*- and *trans*-inhibition, respectively). Kinetic parameters were estimated by a nonlinear least-squares regression analysis based on the Michaelis-Menten equation (*Eq. 2*) and are shown as mean ± SD from three independent experiments.

Assay condition	Preincubation Time (min)	Concentration of CsA (μM)		K_m (μM)	V_{max} (pmol/min/mg protein)
		Preincubation step	[^{3}H]E_2G coincubation step		
Cis-inhibition	NA	NA	0	8.52 ± 1.63	232 ± 37
	NA	NA	0.3	16.9 ± 1.02[a]	241 ± 13
Trans-inhibition	120	0	0	7.47 ± 1.02	241 ± 54
	120	0.01	0	7.77 ± 2.58	167 ± 14[a]

NA, not applicable.
[a]$p < 0.05$ compared with the corresponding control condition.

$K_{i,app}$ values of 0.492 and 0.524 μM after 10- and 60-minute preincubation with rifampin, respectively (Table 1). From the relationship between simulated cellular level of rifampin and observed *trans*-inhibition of OATP1B1 (Fig. 9B), the $K_{i,trans}$ of rifampin was estimated to be 1.56 μM (Table 3). The $K_{i,trans}$ and $K_{i,app}$ values were estimated based on the intracellular unbound concentration and buffer concentration of rifampin, respectively. Intracellular concentration of unbound rifampin is higher than medium concentration due to its active transport mediated by OATP1B1, and $K_{i,trans}$ (1.56 μM) was slightly larger than $K_{i,app,trans}$ (1.01 to 1.39 μM).

Long-lasting inhibition of OATP1B1 after 60-minute preincubation with rifampin at 10 and 100 μM was also investigated (Fig. 9C). OATP1B1 activity immediately recovered within 10 minutes after removing rifampin from buffer, but partially at 100 μM. Using the optimized parameters (Table 3), the recovery of OATP1B1 activity in the long-lasting inhibition assay conditions was also well reproduced by the cellular kinetic model (Fig. 9C). At 100 μM of rifampin, the OATP1B1 activity was recovered only partially, which was due to the amount of rifampin that remains in the cells (exhibit *trans*-inhibition of OATP1B1) even after a 60-minute washout period.

Discussion

In the present study, preincubation time-dependent, long-lasting inhibition of OATP1B1 by CsA and rifampin was characterized in OATP1B1-HEK and control-HEK cells, and the in vitro data were analyzed by kinetic modeling to gain the mechanistic insights and to identify the factors impacting the extent of the preincubation time-dependent inhibition of OATP1B1.

Similar to the previous reports (Pahwa et al., 2017; Barnett et al., 2018), our current results confirmed the differences between CsA and rifampin in terms of preincubation time-dependent shift of $K_{i,app}$ values. Following 120-minute preincubation in *trans*- and *cis*+*trans*-inhibition assay conditions, the inhibitory potency of CsA on OATP1B1 was markedly enhanced: the $K_{i,app}$ values of CsA were decreased by 16.5- and 27.2-fold compared with that in *cis*-inhibition assay conditions, respectively (Fig. 3 and Table 1). Prolonged preincubation (60 minutes or longer) was required for reaching the maximum OATP1B1 inhibition in *trans*-inhibition assay conditions (Fig. 7). On the other hand, the $K_{i,app}$ shift of rifampin was modest (only by twofold) in the *cis*+*trans*-inhibition assay conditions (Fig. 9A and Table 1) and 10-minute preincubation was sufficient to reach the maximum *trans*-inhibition (Fig. 9B). Cellular kinetic modeling predicted that CsA uptake into HEK293 cells reached a steady-state after 60-minute or longer incubation (Fig. 5A) and concentration-dependent cellular distribution (Fig. 5B) via high-affinity, high-capacity intracellular binding (possibly with cyclophilin A). The uptake of rifampin in OATP1B1-HEK was approximately twice that in control-HEK, likely from OATP1B1-mediated uptake with a K_m value of 0.382 μM (Supplemental Fig. 2 and Table 3). In contrast to CsA, the uptake of rifampin reached a steady-state quickly (within 10 minutes) in both OATP1B1-HEK and control-HEK (Supplemental Fig. 2). These results support the association of intracellular inhibitor concentrations with the enhancement of OATP1B1 inhibition in the *trans*- and *cis*+*trans*-inhibition conditions.

The time profiles for the uptake and release of CsA in HEK293 cells were well captured by the cellular kinetic model incorporating saturable intracellular binding (Fig. 6). Based on the experimental data of OATP1B1 inhibition by CsA (Fig. 4), our kinetic model incorporated the components of competitive *cis*-inhibition and noncompetitive *trans*-inhibition (Fig. 2). The model captured the preincubation time-dependency in *trans*-inhibition (Fig. 7) as well as long-lasting inhibition of OATP1B1 by CsA (Fig. 8). The *trans*-inhibition potency of CsA

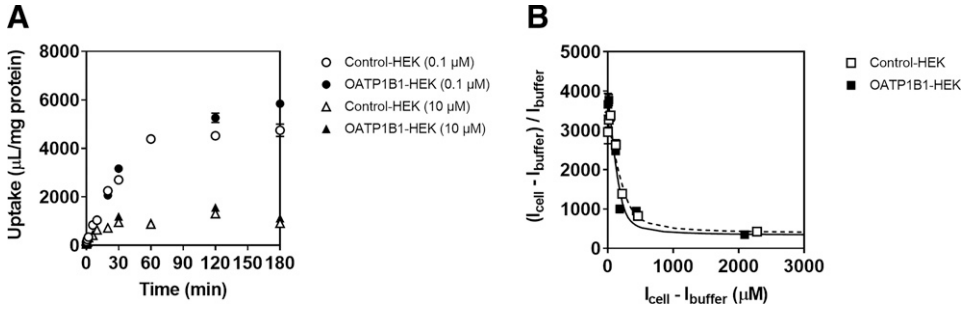

Fig. 5. Time profiles and concentration dependence of the uptake of CsA into HEK293 cells. (A) Uptake of CsA into OATP1B1-HEK (closed symbols) and control-HEK (open symbols) at 0.1 (circles) and 10 μM (triangles) were determined over 180 min at 37°C. Each point represents the mean ± S.E.M. (n = 3). (B) CsA (0.001 – 10 μM) was incubated with OATP1B1-HEK (■) and control-HEK (□) for 120 min at 37°C. The cellular uptake was analyzed by Eq. 3 and the data are shown as a Scatchard plot. Representative data from three independent experiments are presented. Each point represents the mean ± S.E.M. (n = 3).

TABLE 3

Cellular kinetic parameters of CsA and rifampin.

Parameters	Units	Inhibitors	
		CsA	Rifampin
K_d	μM	0.0914 ± 0.0245[a]	NA
B_{max}	μM	326 ± 111[a]	NA
A		362 ± 26[a]	NA
f_T		0.000254[b]	0.0311 ± 0.0009[c]
PS_{dif}	μl/min/mg protein	51.3 ± 13.8[c]	52.5 ± 2.2[c]
V_{max}	pmol/min/mg protein	NA	25.1 ± 6.7[c]
K_m	μM	NA	0.382 ± 0.134[c]
$K_{p,uu}$		1[d]	2.25[e]
$K_{i,cis}$	μM	0.297 ± 0.027[f]	1.16 ± 0.01[f]
$K_{i,trans}$	μM	0.00619 ± 0.00138[c]	1.56 ± 0.10[c]
$K_{i,cis}$-to-$K_{i,trans}$ ratio (α)		48.0	0.744

NA, not available.
[a]Determined by in vitro studies using Eq. 3 (mean ± SD, n=6).
[b]f_T value under linear condition, calculated from K_d, B_{max}, and A.
[c]Estimated by cellular kinetic model fitting (parameter estimate ± parameter SD).
[d]Assumed to be unity.
[e]$K_{p,uu}$ of rifampin was estimated by $(1 + PS_{act}/PS_{dif})$.
[f]Estimated according to Eq. 1 (parameter estimate ± parameter SD).

($K_{i,trans}$, 0.00619 μM) was much stronger than that of *cis*-inhibition ($K_{i,cis}$, 0.297 μM), and the *trans*-inhibition was potentiated as preincubation time-dependent intracellular accumulation of CsA. Our current study offers the experimental validation of the proposed *trans*-inhibition mechanism for OATP1B1 TDI caused by CsA (Shitara and Sugiyama, 2017), differing from the mechanism-based inhibition of drug metabolizing enzymes (Murray, 1997; Lin and Lu, 1998).

Cellular kinetic parameters of CsA and rifampin may provide important insights into the factors impacting the TDI of OATP1B1. For comparison, we calculated the time to reach half maximum intracellular concentration ($T_{1/2,max}$) as follows:

$$T_{1/2,max} = \frac{0.693 \times V_{cell}}{PS_{dif} \times f_T} \quad (10)$$

The calculated $T_{1/2,max}$ values of CsA and rifampin were 106 and 0.849 minutes, respectively. Given the similar PS_{dif} values between CsA and rifampin (Table 3), the large difference in $T_{1/2,max}$ is related to approximately 120-fold lower f_T values of CsA under linear conditions than that of rifampin (Table 3). Other factors to consider are the $K_{i,cis}$-to-$K_{i,trans}$ ratio (α), and intracellular-to-buffer unbound drug concentration ratio ($K_{p,uu}$). According to Eq. 9, intracellular unbound inhibitor concentration ($f_T \cdot I_{cell}$) can be replaced by $K_{p,uu} \cdot I_{buffer}$ at a steady-state. Then,

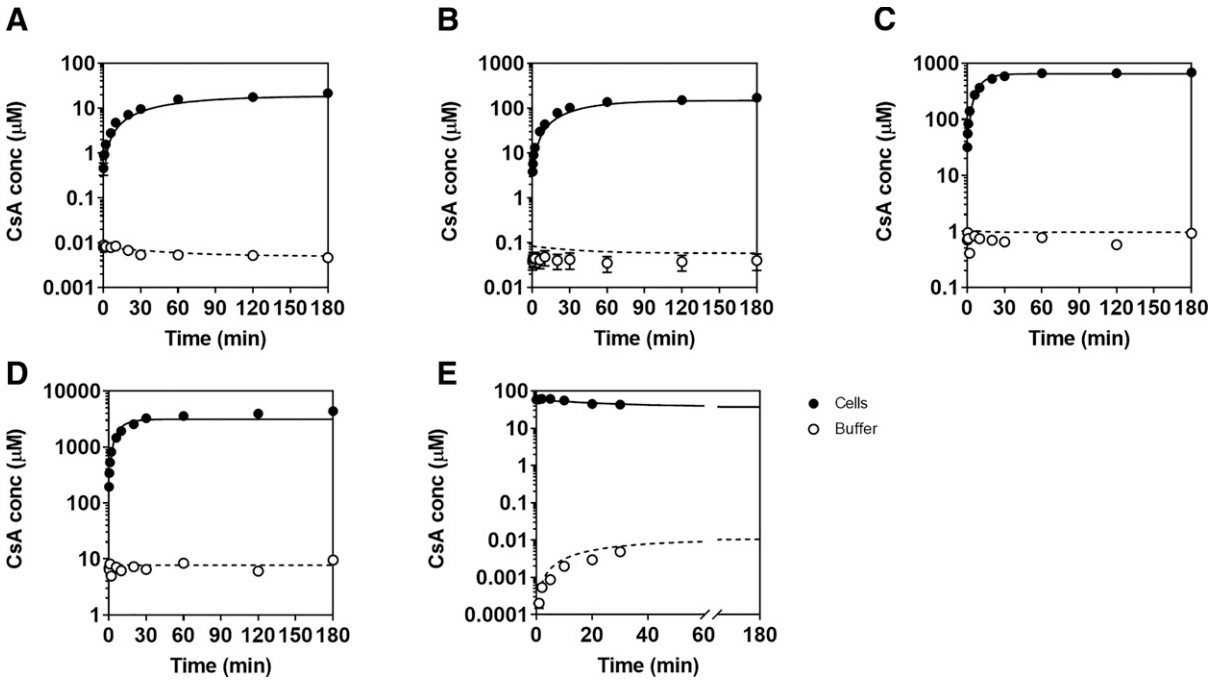

Fig. 6. Time profiles for the uptake and release of CsA in HEK293 cells. Time profiles for the uptake (A–D) and release (E) of CsA were examined in HEK293 cells. Since results were similar between OATP1B1-HEK and control-HEK cells, the data were combined and shown as mean ± S.E.M. (n = 6). (A–D) KH buffer containing CsA at 0.01 (A), 0.1 (B), 1 (C), and 10 (D) μM was incubated with HEK293 cells over 180 min to investigate the uptake of CsA. (E) After the incubation of CsA (0.1 μM) with HEK293 cells for 120 min at 37°C, cells were washed and incubated with KH buffer for 30 min at 37°C to see the release of CsA into the buffer. The cellular (●) and buffer (○) concentrations of CsA were determined by LC-MS/MS. To estimate the PS_{dif} value of CsA, observed intracellular and buffer concentration of CsA were simultaneously fitted to Eqs. 4, 5, and 7 with B_{max} (326 μM), K_d (0.0914 μM), and A (362) as shown in Table 3. Solid and dashed lines represent the fitted lines for cellular and buffer concentrations of CsA.

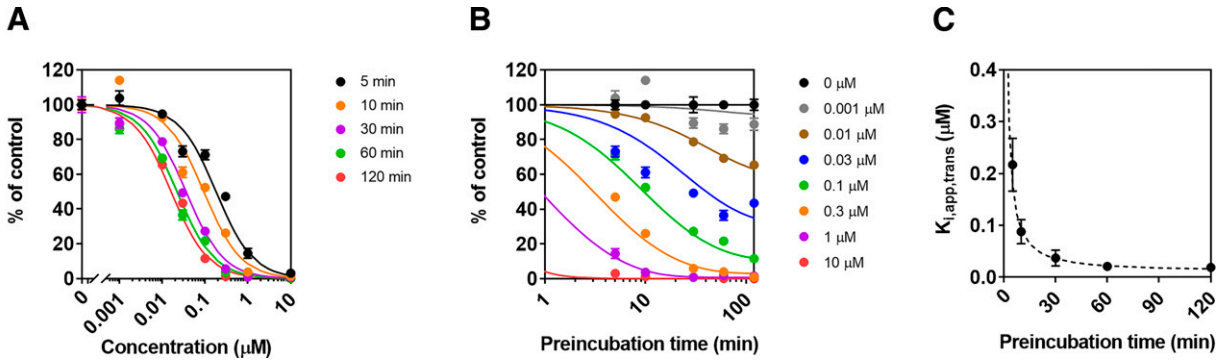

Fig. 7. Observed and simulated profiles for preincubation time dependency in *trans*-inhibition of OATP1B1 by CsA in OATP1B1-HEK cells. (A, B) The preincubation time-dependent inhibition curve shift (A) and potentiation of OATP1B1 inhibition by CsA (B) were examined in vitro. After preincubation with CsA (0.001 – 100 μM) for 5, 10, 30, 60, and 120 min, OATP1B1-mediated uptake of [^{3}H]E_2G (0.1 μM) was determined in the absence of CsA, and observed % of control values (relative to OATP1B1-mediated uptake of [^{3}H]E_2G without CsA preincubation) were presented as closed circles (mean ± S.E.M., n = 3). The observed % of control values were fitted to Eq. 9, where I_{buffer} of CsA was set to zero, and $f_T \cdot I_{cell}$ of CsA simulated by Eqs. 4, 5, and 7 with fixed B_{max} (326 μM), K_d (0.0914 μM), and A (362) as shown in Table 3 was used, setting PS_{dif} as a free parameter. Solid lines in (A) and (B) are fitted lines for % of control values, yielding PS_{dif} and $K_{i,trans}$ values (parameter estimate ± parameter SD) of 51.3 ± 13.8 μl/min/mg protein and 0.00619 ± 0.00138 μM, respectively. (C) The preincubation-time dependent shift of $K_{i,app}$ values observed in the *trans*-inhibition study ($K_{i,app,trans}$) were shown with closed circles (mean ± SD, n = 3), and compared with simulated values. For$K_{i,app,trans}$ simulation (dashed line), the % of control values were estimated by Eq. 9, where I_{buffer} and $K_{i,trans}$ were set to zero and 0.00619 μM, respectively, and $f_T \cdot I_{cell}$ values were simulated by Eqs. 4, 5, and 7 using optimized parameters given in Table 3. Then, the estimated % of control values after CsA preincubation were input into Eq. 1, where nominal CsA concentration in buffer was used as the I_{buffer}.

OATP1B1-mediated uptake clearance is decreased by a factor of $(1+I_{buffer}/K_{i,cis})$ or $(1+ \alpha \cdot K_{p,uu} \cdot I_{buffer}/K_{i,cis})$ in *cis*- or *trans*-inhibition, respectively. Therefore, $\alpha \cdot K_{p,uu}$ is a determinant of the extent of enhancement of OATP1B1 inhibition after preincubation. The $K_{p,uu}$ of rifampin was 2.25 due to active uptake via OATP1B1, but symmetrical *cis*- and *trans*-inhibition of OATP1B1 offered the α value of 0.744, resulting in $\alpha \cdot K_{p,uu}$ of 1.7. Although $K_{p,uu}$ was unity for CsA, the contribution of *trans*-inhibition to the overall OATP1B1 inhibition was much greater than that of *cis*-inhibition, producing the α (and $\alpha \cdot K_{p,uu}$) value of 48. Furthermore, when the OATP1B1-mediated uptake is reduced by 50% in *cis*+*trans*-inhibition study, I_{buffer} is equal to $K_{i,app,cis+trans}$ at a steady-state in Eq. 9, and $K_{i,app,cis+trans}$ can be described as follows:

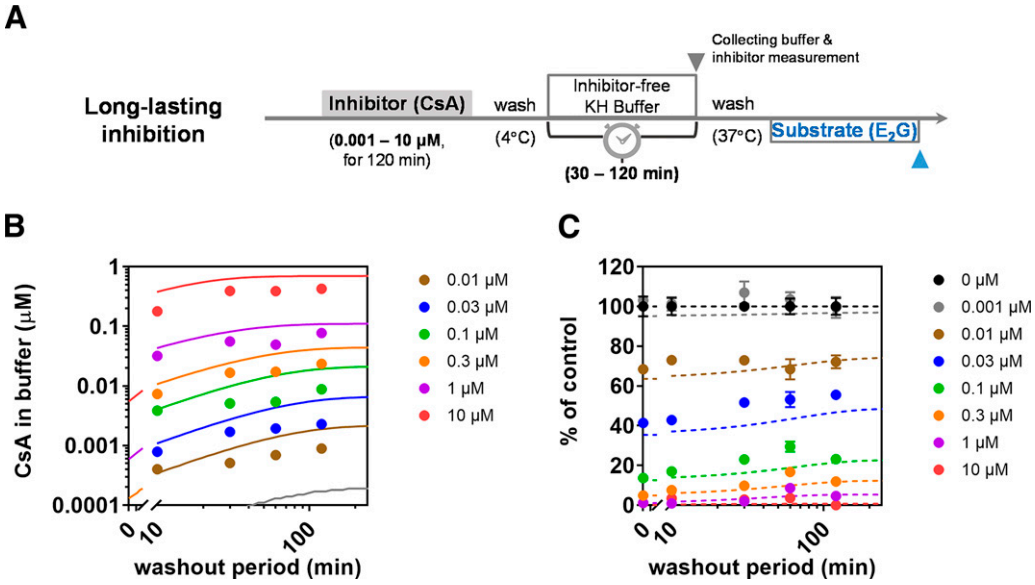

Fig. 8. Observed and simulated long-lasting inhibition of OATP1B1 by cyclosporine A (CsA) in OATP1B1-HEK cells. (A) Assay procedure for long-lasting inhibition of OATP1B1 by CsA. After 120-min preincubation of CsA (0.001–10 μM) at 37°C with OATP1B1-HEK and control-HEK, cells were washed and incubated with 500 μl of fresh KH buffer at 37°C. At the designated times (up to 120 min), buffer samples were collected to measure concentrations of CsA released from the cells into buffer (B), followed by washout. Then, OATP1B1-mediated uptake of [^{3}H]E_2G (0.1 μM) was examined in buffer lacking CsA (C). Closed circles represent the observed data (mean ± S.E.M., n = 6 (B) or 3 (C)). To simulate CsA concentration in buffer and the recovery of OATP1B1 activity, the intracellular concentration (I_{cell}) of CsA after 120-min preincubation with CsA (0.01–10 μM), which was estimated according to Eqs. 4, 5, and 7 using optimized parameters (Table 3), was used as initial value (t = 0). Then, time profiles for concentrations of CsA released from the cells into buffer (I_{buffer}; I_{buffer} = 0 at t = 0) were simulated (solid lines) (B). Since CsA was not measurable in buffer after preincubation of CsA at 0.001 μM, only a simulation line was shown in gray (B). The I_{cell} and f_T values of CsA during washout period were also simulated according to Eqs. 4, 5, and 7 using optimized parameters (Table 3) and input into Eq. 9 with fixed $K_{i,trans}$ (0.00619 μM) and I_{buffer} (0 μM) to simulate the recovery of OATP1B1 activity (% of control values; dashed lines) (C).

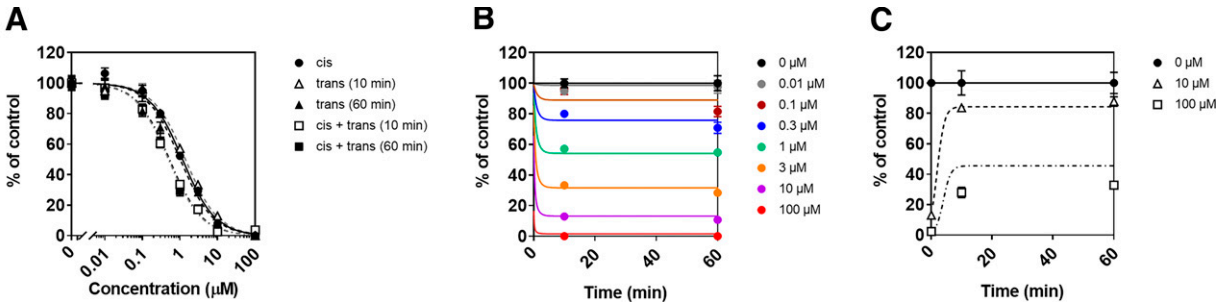

Fig. 9. Preincubation time-dependent inhibition of OATP1B1 by rifampin. (A) Inhibitory effect of rifampin (0.01–100 μM) on OATP1B1-mediated uptake of [^{3}H]E_2G (0.1 μM) was examined in *cis*-, *trans*-, and *cis*+*trans*-inhibition conditions using OATP1B1-HEK and control-HEK. In the *cis*-inhibition condition, rifampin and [^{3}H]E_2G were coincubated without preincubation with rifampin (●). In the *trans*-inhibition condition, [^{3}H]E_2G uptake was examined after 10- (△) or 60-min (▲) preincubation with rifampin. In the *cis*+*trans*-inhibition condition, rifampin and [^{3}H]E_2G were coincubated after 10- (□) or 60-min (■) preincubation with rifampin. Each symbol represents mean ± S.E.M. (n=3), and solid (*cis*-inhibition), dashed (*trans*-inhibition), and dash-dotted lines (*cis*+*trans*-inhibition) represent fitted lines obtained according to Eq. 1. (B) *Trans*-inhibition of OATP1B1 by rifampin. After preincubation with rifampin (0.01–100 μM) for 10 and 60 min, OATP1B1-mediated uptake of [^{3}H]E_2G (0.1 μM) was determined in buffer lacking rifampin, and observed % of control values (relative to OATP1B1-mediated uptake of [^{3}H]E_2G without rifampin preincubation) were presented as closed circles (mean ± S.E.M., n=3). The observed % of control values were fitted to Eq. 9, where I_{buffer} of rifampin was set to zero, and $f_T \cdot I_{cell}$ of rifampin that was simulated by Eqs. 4, 5, and 6 with fixed PS_{dif} (52.5 μl/min/mg protein), V_{max} (25.1 pmol/min/mg protein), K_m (0.382 μM), and f_T (0.0311 μM) as shown in Table 3 was used. Solid lines represent fitted lines for % of control values, yielding estimated $K_{i,trans}$ value (parameter estimate ± parameter SD) of 1.56 ± 0.10 μM. (C) Long-lasting inhibition of OATP1B1-mediated uptake of [^{3}H]E_2G (0.1 μM) by rifampin (10 and 100 μM) was examined using OATP1B1-HEK and control-HEK. After 60-min preincubation of rifampin at 0 (●), 10 (△), and 100 μM (□) with OATP1B1-HEK and control-HEK, cells were washed and incubated with 500 μl of fresh KH buffer at 37°C. At 10- and 60-min washout period, buffer was removed, followed by washing cells. Then, OATP1B1-mediated uptake of [^{3}H]E_2G was examined in buffer lacking rifampin. Each symbol represents observed value (mean ± S.E.M., n=3). To simulate the recovery of OATP1B1 activity, the intracellular concentration (I_{cell}) of rifampin after 60-min preincubation with rifampin (10 and 100 μM), which was estimated according to Eqs. 4, 5, and 6 using optimized parameters (Table 3), was used as initial value (t = 0). Then, the I_{cell} of rifampin during washout period were simulated according to Eqs. 4, 5, and 6 using optimized parameters (Table 3) and input into Eq. 9 with fixed $K_{i,trans}$ (1.56 μM), f_T (0.0311), and I_{buffer} (0 μM) to simulate the recovery of OATP1B1 activity (% of control values). Solid, dashed, and dash-dotted lines represent simulated % control values after 60-min preincubation with rifampin at 0, 10, and 100 μM, respectively.

$$K_{i,app,cis+trans} = \left[\sqrt{\left\{(1+K_{p,uu}\cdot\alpha)/K_{i,cis}\right\}^2 + 4\cdot K_{p,uu}\cdot\alpha/{K_{i,cis}}^2} - \left\{(1+K_{p,uu}\cdot\alpha)/K_{i,cis}\right\}\right]/\left(2\cdot\alpha\cdot K_{p,uu}/{K_{i,cis}}^2\right) \quad (11)$$

The derivation of Eq. 11 is given in the supplemental text. Based on this equation, simulations were performed to assess the impact of α and $K_{p,uu}$ on the steady-state $K_{i,app,cis+trans}$ for CsA (Supplemental Figs. 3, A and B) and rifampin (Supplemental Figs. 3, C and D): for both drugs, the larger α and $K_{p,uu}$ values, the smaller $K_{i,app,cis+trans}$ values. Together, it is likely that the long $T_{1/2,max}$ and large $\alpha \cdot K_{p,uu}$ of CsA account for notable preincubation time-dependent potentiation of OATP1B1 inhibition compared with rifampin.

The cellular kinetic model of CsA (Fig. 2 and Table 3) was also used for the sensitivity analysis examining the impact of PS_{dif}, f_T, $K_{p,uu}$, and $K_{i,trans}$ on the cellular PK and preincubation time-dependent change in $K_{i,app,cis+trans}$ and $K_{i,app,trans}$ (Fig. 10 and Supplemental Fig. 4). Simulation results indicated that the smaller PS_{dif} (Fig. 10, A and B) or f_T (Supplemental Fig. 4), the longer preincubation time to reach a steady-state in $I_{cell,u}$ and maximum *trans*- and *cis*+*trans*-inhibition. With a sufficiently long time, $I_{cell,u}$ would correspond to I_{buffer} (regardless of PS_{dif} or f_T values) and $K_{i,app,cis+trans}$ to $K_{i,app,trans}$ at a steady-state. The greater $K_{p,uu}$ values, the higher $I_{cell,u}$ values (Fig. 10C), and the more potent *trans*- and *cis*+*trans*-inhibition (Fig. 10D). In Figs. 10, E and F, the contribution of *trans*-inhibition relative to *cis*-inhibition was reduced by increasing $K_{i,trans}$ to 10 and 48 times the original values (i.e., $K_{i,cis}$ = 48 × $K_{i,trans}$). Overall OATP1B1 inhibition was accounted for by *cis*- and *trans*-inhibition, but preincubation time-dependent shift of $K_{i,app,cis+trans}$ values was less pronounced. The simulation results suggest that $T_{1/2,max}$ and $\alpha \cdot K_{p,uu}$ are key parameters determining the degree of preincubation time-dependency of OATP1B1 inhibitors and may collectively influence optimal preincubation time in evaluating OATP1B1 inhibition at steady-state. Further investigation is warranted to conclude whether the current findings are applicable to preincubation effect-positive OATP1B1 inhibitors other than CsA.

The preincubation effects have also been observed in other solute carrier (SLC) transporters such as OATP1B3, organic anion transporter 1, organic anion transporter 3, organic cation transporter 1, organic cation transporter 2, multidrug and toxin extrusion protein 1, multidrug and toxin extrusion protein 2K, and Na+-taurocholate cotransporting polypeptide (NTCP) (Gertz et al., 2013; Furihata et al., 2014; Ma et al., 2015; Arakawa et al., 2017; Oh et al., 2018; Omote et al., 2018; Tátrai et al., 2019; Lowjaga et al., 2020). Tátrai et al. comprehensively examined preincubation-dependency for the inhibition of clinically relevant SLC transporters (Tátrai et al., 2019). In their report, in the case of the inhibitors displaying the enhancement by preincubation, it took a long time to reach equilibrium between intracellular concentration and buffer concentrations. In contrast, rapid equilibrium was achieved for preincubation effect-negative inhibitors (Tátrai et al., 2019). Recently, Lowjaga et al. reported that taurolithocholic acid exhibited long-lasting *trans*-inhibition of NTCP and discussed the physiologic significance of the NTCP *trans*-inhibition mechanism as a potential defense system to protect hepatocytes from cholestatic bile acids and the hepatitis B and D virus infection (Lowjaga et al., 2020). The inhibition profiles reported with various SLC transporters appear consistent with the TDI mechanism of OATP1B1, and *trans*-inhibition may be a common phenomenon for SLC transporters with different intracellular retention mechanisms of inhibitors, such as on-target (e.g., cyclophilin A) or off-target intracellular binding, lysosomal trapping, and/or active uptake of inhibitors. The in vitro experimental protocols and kinetic modeling approach employed in the current study may aid in elucidating the TDI mechanism of additional SLC transporters.

Another implication of the current findings may be for the risk assessment of OATP1B1-mediated DDIs. Regulatory DDI guidelines recommend that K_i values for OATP1B1 and OATP1B3 be determined after preincubation with NCEs (MHLW, 2019; U.S. FDA, 2020). Since the $T_{1/2,max}$ values depend on the PS_{dif} and f_T values of a given compound (Fig. 10 and Supplemental Fig. 4), preincubation time needs to be optimized for each compound. In the clinical DDIs, the inhibitor

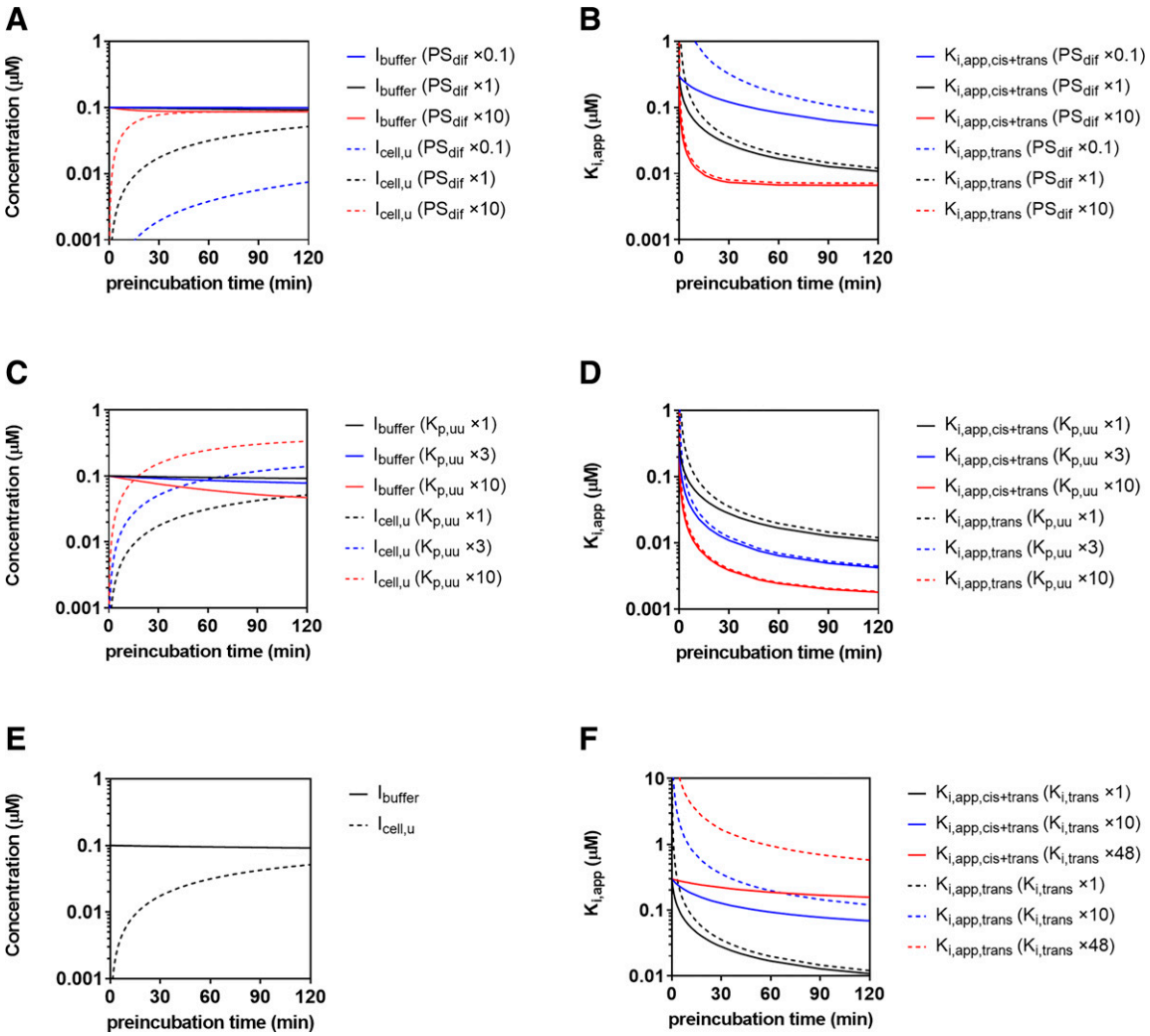

Fig. 10. Simulation of the impact of PS_{dif}, $K_{p,uu}$, and α on the cellular pharmacokinetics and preincubation-time dependent shift of $K_{i,app,cis+trans}$ and $K_{i,app,trans}$ of CsA. The impacts of PS_{dif} (A and B), $K_{p,uu}$ (C and D), and α ($K_{i,cis}$-to-$K_{i,trans}$ ratio; E and F) on the time profiles for I_{buffer} and $I_{cell,u}$ of CsA (initial value for I_{buffer}, 0.1 μM; A, C, and E) during preincubation period and preincubation time-dependent shift of $K_{i,app,cis+trans}$ and $K_{i,app,trans}$ values (B, D, and F) were simulated up to 120 min. The cellular pharmacokinetic parameters of cyclosporine A shown in Table 3 were used as default values, and cellular protein amount was set to 0.01 mg protein/well in these simulations to minimize the impact on I_{buffer}. (A and B) To see the impact of $T_{1/2,max}$, PS_{dif} value was set to 5.13 (PS_{dif} × 0.1), 51.3 (PS_{dif} × 1, default value), and 513 (PS_{dif} × 10) μl/min/mg protein, keeping f_T constant (0.000254). (C and D) To simulate the situations with $K_{p,uu}$ values of 1, 3, and 10, PS_{act} value was set to 0 (default value), 103, and 462 μl/min/mg protein, respectively, keeping PS_{dif} constant (51.3 μl/min/mg protein). (E and F) To see the effect of α ($K_{i,cis}$-to-$K_{i,trans}$ ratio) values at 48, 4.8, and 1, $K_{i,trans}$ value was set to 0.00619 ($K_{i,trans}$ × 1, default value), 0.0619 ($K_{i,trans}$ × 10), and 0.297 ($K_{i,trans}$ × 48, equal to $K_{i,cis}$) μM, respectively, keeping $K_{i,cis}$ constant (0.297 μM).

drugs are distributed to the liver and expected to access OATP1B1 from extracellular (plasma) and intracellular (liver) sides. In that regard, the use of steady-state $K_{i,app,cis+trans}$ values may be more relevant to in vivo situations and desirable to avoid false-negative DDI predictions by the static model. However, it should be noted that the unbound concentrations of the inhibitor in the plasma and liver should change with time in vivo, and the use of steady-state $K_{i,app,cis+trans}$ based on the unbound inhibitor concentration in buffer may overestimate the extent of in vivo DDI. To overcome this difficulty, the mechanistic PBPK models involving *cis*- and *trans*-inhibition taking into the account the time-dependent change in the unbound inhibitor concentrations in the blood and liver should be established in the near future.

In conclusion, we experimentally validated the underlying mechanism for preincubation-dependent, long-lasting inhibition of OATP1B1 by CsA, in which the extensive intracellular binding and *cis*- and *trans*-inhibition of OATP1B1 were found to be key drivers. OATP1B1 inhibitors with long $T_{1/2,max}$, and large $K_{i,cis}$-to-$K_{i,trans}$ ratio and $K_{p,uu}$ could show a significant preincubation effect in the in vitro inhibition assays. This study provided a mechanistic understanding of the TDI of OATP1B1 in vitro, contributing to more accurate, quantitative prediction of transporter-mediated DDIs and developing safer medicines for patients.

Acknowledgments

The authors sincerely thank Soo-Jin Kim (Biome Research Laboratory, Korea Kolmar Holdings Co., Ltd.), Kota Toshimoto (Astellas Pharma, Inc.), and Takashi Yoshikado (Yokohama University of Pharmacy) for invaluable suggestions and technical support.

Authorship Contributions

Participated in research design: Izumi, Sugiyama.
Conducted experiments: Izumi.
Performed data analysis: Izumi, Nozaki.
Wrote or contributed to the writing of the manuscript: Izumi, Nozaki, Lee, Sugiyama.

References

Amundsen R, Christensen H, Zabihyan B, and Åsberg A (2010) Cyclosporine A, but not tacrolimus, shows relevant inhibition of organic anion-transporting protein 1B1-mediated transport of atorvastatin. *Drug Metab Dispos* **38**:1499–1504.

Arakawa H, Omote S, and Tamai I (2017) Inhibitory effect of crizotinib on creatinine uptake by renal secretory transporter OCT2. *J Pharm Sci* **106**:2899–2903.

Barnett S, Ogungbenro K, Ménochet K, Shen H, Lai Y, Humphreys WG, and Galetin A (2018) Gaining mechanistic insight into coproporphyrin I as endogenous biomarker for OATP1B-mediated drug-drug interactions using population pharmacokinetic modeling and simulation. *Clin Pharmacol Ther* **104**:564–574.

Dalgarno DC, Harding MW, Lazarides A, Handschumacher RE, and Armitage IM (1986) 1H NMR studies on bovine cyclophilin: preliminary structural characterization of this specific cyclosporin A binding protein. *Biochemistry* **25**:6778–6784.

Furihata T, Matsumoto S, Fu Z, Tsubota A, Sun Y, Matsumoto S, Kobayashi K, and Chiba K (2014) Different interaction profiles of direct-acting anti-hepatitis C virus agents with human organic anion transporting polypeptides. *Antimicrob Agents Chemother* **58**:4555–4564.

Gertz M, Cartwright CM, Hobbs MJ, Kenworthy KE, Rowland M, Houston JB, and Galetin A (2013) Cyclosporine inhibition of hepatic and intestinal CYP3A4, uptake and efflux transporters: application of PBPK modeling in the assessment of drug-drug interaction potential. *Pharm Res* **30**:761–780.

Hisaka A and Sugiyama Y (1998) Analysis of nonlinear and nonsteady state hepatic extraction with the dispersion model using the finite difference method. *J Pharmacokinet Biopharm* **26**:495–519.

Iwaki Y, Lee W, and Sugiyama Y (2019) Comparative and quantitative assessment on statin efficacy and safety: insights into inter-statin and inter-individual variability via dose- and exposure-response relationships. *Expert Opin Drug Metab Toxicol* **15**:897–911.

Izumi S, Nozaki Y, Komori T, Maeda K, Takenaka O, Kusano K, Yoshimura T, Kusuhara H, and Sugiyama Y (2013) Substrate-dependent inhibition of organic anion transporting polypeptide 1B1: comparative analysis with prototypical probe substrates estradiol-17β-glucuronide, estrone-3-sulfate, and sulfobromophthalein. *Drug Metab Dispos* **41**:1859–1866.

Izumi S, Nozaki Y, Maeda K, Komori T, Takenaka O, Kusuhara H, and Sugiyama Y (2015) Investigation of the impact of substrate selection on in vitro organic anion transporting polypeptide 1B1 inhibition profiles for the prediction of drug-drug interactions. *Drug Metab Dispos* **43**:235–247.

Ke H, Mayrose D, Belshaw PJ, Alberg DG, Schreiber SL, Chang ZY, Etzkorn FA, Ho S, and Walsh CT (1994) Crystal structures of cyclophilin A complexed with cyclosporin A and N-methyl-4-[(E)-2-butenyl]-4,4-dimethylthreonine cyclosporin A. *Structure* **2**:33–44.

Kuglstatter A, Mueller F, Kusznir E, Gsell B, Stihle M, Thoma R, Benz J, Aspeslet L, Freitag D, and Hennig M (2011) Structural basis for the cyclophilin A binding affinity and immunosuppressive potency of E-ISA247 (voclosporin). *Acta Crystallogr D Biol Crystallogr* **67**:119–123.

Lin JH and Lu AY (1998) Inhibition and induction of cytochrome P450 and the clinical implications. *Clin Pharmacokinet* **35**:361–390.

Lowjaga KAAT, Kirstgen M, Müller SF, Goldmann N, Lehmann F, Glebe D, and Geyer J (2020) Long-term trans-inhibition of the hepatitis B and D virus receptor NTCP by taurolithocholic acid. *Am J Physiol Gastrointest Liver Physiol.* **320**:G66–G80.

Ma L, Qin Y, Shen Z, Hu H, Zhou H, Yu L, Jiang H, and Zeng S (2015) Time-dependent inhibition of hOAT1 and hOAT3 by anthraquinones. *Biol Pharm Bull* **38**:992–995.

Maeda K (2015) Organic anion transporting polypeptide (OATP)1B1 and OATP1B3 as important regulators of the pharmacokinetics of substrate drugs. *Biol Pharm Bull* **38**:155–168.

Marks WH, Harding MW, Handschumacher R, Marks C, and Lorber MI (1991) The immunochemical distribution of cyclophilin in normal mammalian tissues. *Transplantation* **52**:340–345.

MHLW (2019) Guideline on drug interaction for drug development and appropriate provision of information.

Murray M (1997) Drug-mediated inactivation of cytochrome P450. *Clin Exp Pharmacol Physiol* **24**:465–470.

Neuvonen PJ, Niemi M, and Backman JT (2006) Drug interactions with lipid-lowering drugs: mechanisms and clinical relevance. *Clin Pharmacol Ther* **80**:565–581.

Niemi M, Pasanen MK, and Neuvonen PJ (2011) Organic anion transporting polypeptide 1B1: a genetically polymorphic transporter of major importance for hepatic drug uptake. *Pharmacol Rev* **63**:157–181.

Oh Y, Jeong Y-S, Kim M-S, Min JS, Ryoo G, Park JE, Jun Y, Song Y-K, Chun S-E, Han S, et al. (2018) Inhibition of organic anion transporting polypeptide 1B1 and 1B3 by betulinic acid: Effects of preincubation and albumin in the media. *J Pharm Sci* **107**:1713–1723.

Omar MA and Wilson JP (2002) FDA adverse event reports on statin-associated rhabdomyolysis. *Ann Pharmacother* **36**:288–295.

Omote S, Matsuoka N, Arakawa H, Nakanishi T, and Tamai I (2018) Effect of tyrosine kinase inhibitors on renal handling of creatinine by MATE1. *Sci Rep* **8**:9237.

Pahwa S, Alam K, Crowe A, Farasyn T, Neuhoff S, Hatley O, Ding K, and Yue W (2017) Pretreatment with rifampicin and tyrosine kinase inhibitor dasatinib potentiates the inhibitory effects toward OATP1B1- and OATP1B3-mediated transport. *J Pharm Sci* **106**:2123–2135.

Quesniaux VF, Schreier MH, Wenger RM, Hiestand PC, Harding MW, and Van Regenmortel MH (1988) Molecular characteristics of cyclophilin-cyclosporine interaction. *Transplantation* **46**(2, Suppl)23S–28S.

Ryffel B, Woerly G, Greiner B, Haendler B, Mihatsch MJ, and Foxwell BM (1991) Distribution of the cyclosporine binding protein cyclophilin in human tissues. *Immunology* **72**:399–404.

Sarris AH, Harding MW, Jiang TR, Aftab D, and Handschumacher RE (1992) Immunofluorescent localization and immunochemical determination of cyclophilin-A with specific rabbit antisera. *Transplantation* **54**:904–910.

Shitara Y and Sugiyama Y (2017) Preincubation-dependent and long-lasting inhibition of organic anion transporting polypeptide (OATP) and its impact on drug-drug interactions. *Pharmacol Ther* **177**:67–80.

Shitara Y, Takeuchi K, Nagamatsu Y, Wada S, Sugiyama Y, and Horie T (2012) Long-lasting inhibitory effects of cyclosporin A, but not tacrolimus, on OATP1B1- and OATP1B3-mediated uptake. *Drug Metab Pharmacokinet* **27**:368–378.

Taguchi T, Masuo Y, Futatsugi A, and Kato Y (2020) Static model-based assessment of OATP1B1-mediated drug interactions with preincubation-dependent inhibitors based on inactivation and recovery kinetics. *Drug Metabolism and Disposition* **48**:750–758.

Taskar KS, Pilla Reddy V, Burt H, Posada MM, Varma M, Zheng M, Ullah M, Emami Riedmaier A, Umehara KI, Snoeys J, et al. (2020) Physiologically-based pharmacokinetic models for evaluating membrane transporter mediated drug-drug interactions: Current capabilities, case studies, future opportunities, and recommendations. *Clin Pharmacol Ther* **107**:1082–1115.

Tátrai P, Schweigler P, Poller B, Domange N, de Wilde R, Hanna I, Gáborik Z, and Huth F (2019) A systematic in vitro investigation of the inhibitor preincubation effect on multiple classes of clinically relevant transporters. *Drug Metab Dispos* **47**:768–778.

U.S. FDA (2020) *In Vitro Drug Interaction Studies — Cytochrome*, p 450, Enzyme- and Transporter-Mediated Drug Interactions Guidance for Industry.

Yoshida K, Maeda K, and Sugiyama Y (2012) Transporter-mediated drug–drug interactions involving OATP substrates: predictions based on in vitro inhibition studies. *Clin Pharmacol Ther* **91**:1053–1064.

Yoshikado T, Yoshida K, Kotani N, Nakada T, Asaumi R, Toshimoto K, Maeda K, Kusuhara H, and Sugiyama Y (2016) Quantitative analyses of hepatic OATP-mediated interactions between statins and inhibitors using PBPK modeling with a parameter optimization method. *Clin Pharmacol Ther* **100**:513–523.

Address correspondence to: Dr. Saki Izumi, Global Drug Metabolism and Pharmacokinetics, Tsukuba Research Laboratories, Eisai Co., Ltd., 5-1-3 Tokodai, Tsukuba, Japan. E-mail: s-izumi@hhc.eisai.co.jp